Bull Earthquake Eng (2010) 8:483–499
DOI 10.1007/s10518-009-9121-x

ORIGINAL RESEARCH PAPER

HVSR of ambient noise in Ston (Croatia): comparison with theoretical spectra and with the damage distribution after the 1996 Ston-Slano earthquake

Marijan Herak · Ivo Allegretti · Davorka Herak · Krešimir Kuk · Vlado Kuk · Krešimir Marić · Snježana Markušić · Josip Stipčević

Received: 9 January 2009 / Accepted: 30 April 2009 / Published online: 15 May 2009

Abstract Horizontal-to-vertical spectral ratios (HVSR) of ambient vibrations measured in the ancient town of Ston (Croatia) on 99 locations, are shown to be well matched to the theoretical ones computed for body-waves as well as for the surface waves. This match is poorer for sites on the slopes of nearby hills. The ratios of measured peak horizontal ground acceleration during the damaging earthquake in 1996 ($M_L = 6.0$) and the ones obtained using empirical attenuation laws is approximately equal to the mapped value of the dynamic amplification factor determined on the basis of observed HVSR in the vicinity of the accelerometric station. The HVSR of the accelerogram is very similar to the HVSR of the ambient noise. The damage to the building stock in the old town centre caused by the earthquake series of 1996 is closely related to the estimated soil amplification and its fundamental frequency. More measurements in buildings are needed to arrive at confident conclusions about possible soil-structure resonance.

Keywords Ambient noise · Soil structure · Amplification · Microzonation · HVSR

1 Introduction

The city of Ston is located about 50 km to the NW of Dubrovnik, in southern Dalmatia (Fig. 1). It is a small town with rich history, known for the ancient salterns and the third longest fortification walls in the world. As a part of the Dubrovnik Republic, Ston was also one of the first townships in this part of the world that developed according to the strict urban code enforced from the fourteenth century. It lies on the southern side of the Pelješac peninsula, close to the mainland, at the foothills of the Bartolomija and Supava hills to the north and east, respectively. To the south lies the shallow bay of the Adriatic Sea and a complex of salt-pans. Fertile Ston karst field is located to the east.

M. Herak (✉) · I. Allegretti · D. Herak · K. Kuk · V. Kuk · K. Marić · S. Markušić · J. Stipčević
Department of Geophysics, Faculty of Sciences and Mathematics, University of Zagreb,
Horvatovac 95, 10000 Zagreb, Croatia
e-mail: herak@irb.hr

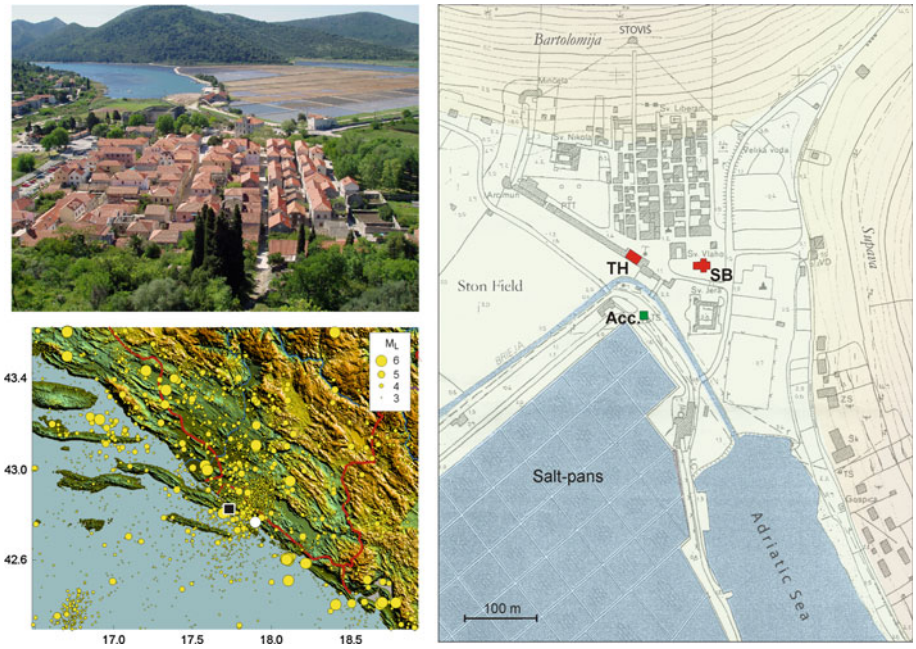

Fig. 1 *Top left* View (N → S) of the Ston centre from the Stoviš tower on the Bartolomija hill (see plan on the *right*). The salt-pans are seen at the top right part of the photo (taken by D. Herak in 2006); *Bottom left* Epicentral map of the greater Ston region (BC-2008, updated catalogue from Herak et al. 1996). Ston is marked by a *black square, white circle* is the epicentre of the 1996 mainshock ($M_L = 6.0$); *Right* Plan of Ston. *TH* Town Hall, *SB* St. Blasius church, *Acc* accelerographic station

Earthquakes are frequent there (Fig. 1). The most recent devastating one occurred in 1996 ($M_L = 6.0$, intensity VIII° MCS in Ston at epicentral distance of 16 km), after which Ston needed almost a decade to recover. Detailed damage survey was done after the earthquake, and reports are available in the archives. The peak horizontal acceleration for the mainshock in Ston exceeded 64% of g and is the highest ever recorded in Croatia.

Here, we report results of the measurements of ambient noise on a dense network of measurement sites (Fig. 3), and compare our findings to the soil structure and damage distribution revealed by previous investigations.

2 Previous studies

Detailed geophysical and geotechnical investigations were carried out in the course of microzonation of Ston by the staff of the IZIIS, Skopje (Aleksovski et al. 1987), who performed borehole measurements and detailed shallow refraction seismic profiling (P and S waves) along 27 profiles with lengths between 75 and 200 m. Interpretation of seismic and borehole data lead to definitions of five layers/geological units, as presented in Table 1.

Our spatial interpolation of data presented in Aleksovski et al. (1987) lead to maps of the depth to the bottom of the first four layers, as presented in Fig. 2. The results clearly indicate thickening of the sedimentary cover as one goes from the Bartolomija hill towards the salt-pans in the south, where total thickness of sediments over the bedrock reaches about 50 m. In the north, only a thin layer of vegetative soil covers the bedrock, which outcrops at numerous places on the Bartolomija hill.

Table 1 Main geological layers deduced from shallow refraction and borehole measurements performed by Aleksovski et al. (1987)

Layer	Composition	v_p (m/s)	v_s (m/s)	ρ (kg/m^3)	D (m)
1	Heterogeneous layer—crushed rocks, clay	300–1250	100–350	1800	1–7
2	Clay with powder and organic impurities; thin layers of mud and peat	700–1400	230–430	1800	4–10
3	Diluvial clay, terra rossa	1000–1780	350–650	1900	5–35
4	Cracked dolomitic limestone, limestone	1780–3100	630–1300	2000	5–52
5	Compact dolomitic limestone and limestone	3650–4700	1640–2340	2400	–

v_p, P-wave velocity; v_s, S-wave velocity; ρ, density; D, depth interval

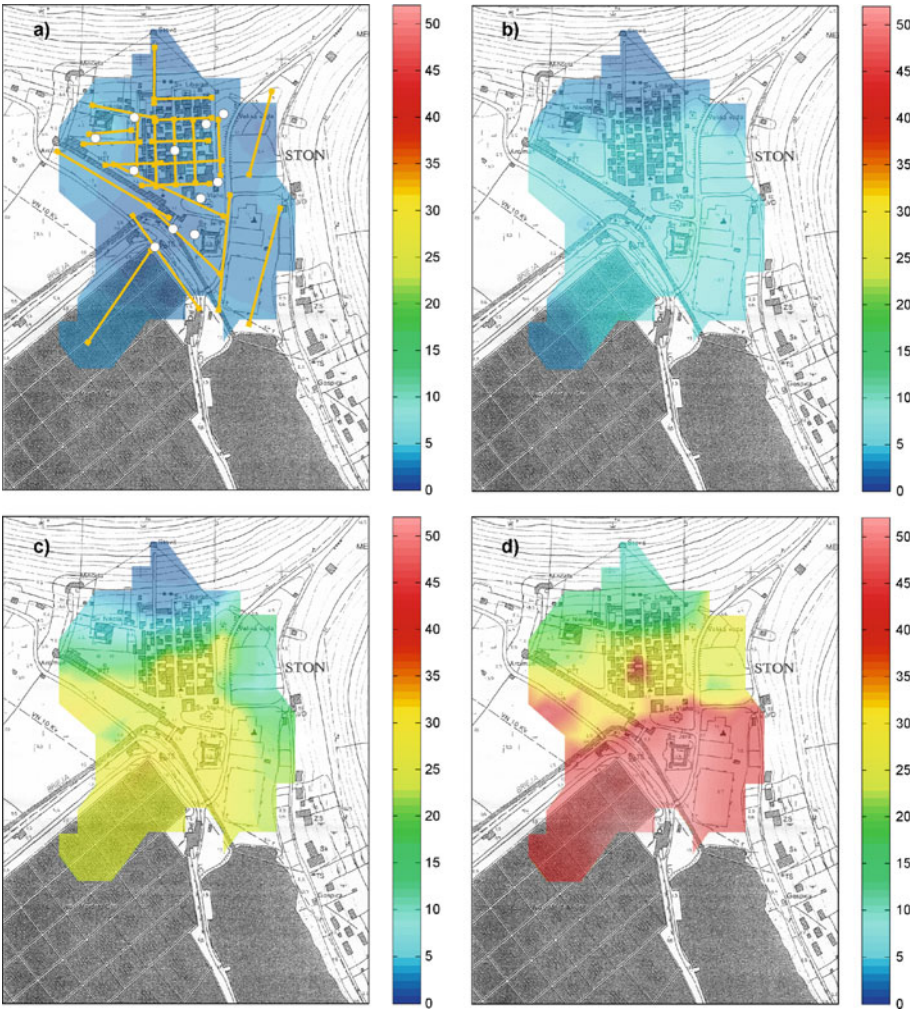

Fig. 2 Maps of interpolated depths (m) to the bottom of layers 1–4 (**a**–**d**, respectively), from Table 1, based on interpreted refraction profiles and boreholes (*orange lines* and *white circles* in subplot **a**, respectively) of Aleksovski et al. (1987)

Table 2 Properties of the first 15 m of soil at the St. Blasius church location (see Fig. 1), determined by Geotehnički studio (2005)

Layer	Composition	N_{SPT}	v_s (m/s)	ρ (kg/m^3)	h (m)
1	Heterogeneous clay of intermediate plasticity, powder, with fractions of sand and pebble;	–	–	1900–1950	2–5
2	Grey soft clay of high plasticity; homogeneous mud with red-brown clay	1–4	76 ± 31–117 ± 42	1900	3–6
3	Red-to-brown clay of high plasticity and solid consistency	12–16	169 ± 57–187 ± 62	1900–2000	>7–8

N_{SPT}, range of number of blows in SPT; v_s, range of shear-wave velocity estimated from 13 relations of v_s as a function of N_{SPT} given in Hasancebi and Ulusay (2006); ρ, density; h, thickness of the layer. Water table is found at 0.7 m depth

In 2005, Geotehnički studio drilled four, 15 m deep, exploration boreholes in the centre of Ston. Their geotechnical study was done for the purpose of reconstruction of the St. Blasius (Sv. Vlaho) church ruined in the 1996 earthquake. The cores reveal a 3-layered structure, summarized in Table 2. The plasticity index of clay ranges between 26 and 41 for the depth range 1–12 m. The water table was shallow (0.7 m) and soil was mostly saturated with water.

The three layers identified by the two groups are seen to have similar physical composition, thickness and density. The shear-wave velocities, however, are different, and those estimated from the Geotehnički studio (2005) data are close to the lower bounds given by Aleksovski et al. (1987). Such values are also in agreement with average velocities that are reported for clays at small depths (e.g. Elnashai and DiSarno 2008). In further theoretical modelling we'll therefore adopt the model of Aleksovski et al. (1987) from Table 1 and Fig. 2, with shear-wave velocities equal to their lower bounds.

According to Eurocode-8 and data from Tables 1 and 2, the soil in Ston may be classified to ground types A (on slopes of the hills), C, D and, due to high plasticity of clay and water saturation, probably also to S1.

3 Measurements

Following the Nakamura (1989) paper on the spectral ratio of horizontal and vertical components (HVSR) of microtremors, ambient noise measurements have become very popular in site-specific investigations and in microzonation studies (e.g. Lachet et al. 1996; Scherbaum et al. 2003; Panou et al. 2005; Havenith et al. 2007; Gosar 2007; Cara et al. 2008; D'Amico et al. 2008; Gosar and Martinec 2009 and papers in Mucciarelli et al. 2009a). The method is attractive as it offers valuable data on soil properties at relatively low-cost. The SESAME project (http://sesame-fp5.obs.ujf-grenoble.fr) produced a number of papers, documents and guidelines regarding measurements and implementation of the method. While there seems to be a consensus that Horizontal-to-vertical spectral ratios (HVSR) peaks reliably identify (at least) fundamental soil frequency, still no agreement is achieved on how to interpret HVSR amplitudes, and how to relate spectra to soil amplification.

Ambient noise measurements in Ston were conducted in three campaigns in May 2006, September 2006, and October 2008. A total of 99 free-field locations were measured, as

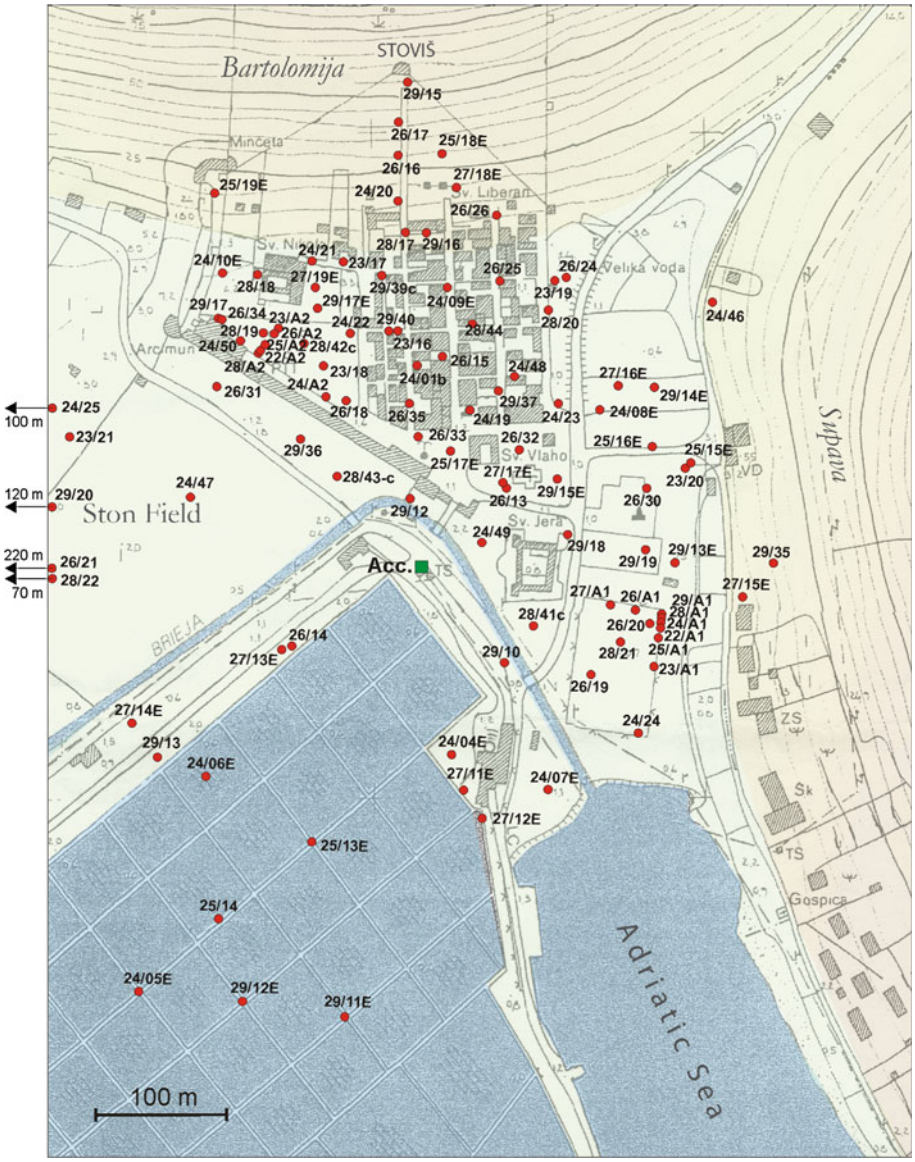

Fig. 3 Map of locations of 99 measurement points (four points plotted at the left edge are outside of the map at distance due east indicated below each *arrow*)

shown in Fig. 3. During all measurements the weather was nice, with low winds. The instruments used were the portable Trominos produced by Micromed, Italy. These are small, all-in-one package seismographs equipped with 3-component geophones, a digitizer, GPS-timing, batteries, and 512 MB flash memory for storage. In the first two campaigns, Trominos were coupled to the ground using one of the two sets of feet (spikes) supplied by the manufacturer. Due to the difficulties experienced in levelling the instruments and to often inadequate coupling to the soil, in the third batch of measurements Trominos (with short

spikes) were put on a granite slate which was firmly laid upon the sand-cushion placed on the ground. This setup enables easy levelling and yields very stable measurements. This is in agreement with experimental results of Chatelain et al. (2008) which suggest that sand provides good ground-instrument coupling with no adverse influence on the measured spectra.

Each measurement lasted for 20 min, and three orthogonal components of noise velocity were recorded at 128 sps. The records were processed using the Grilla (Micromed) software. Each record was first divided into 40 non-overlapping windows. The windows where the ratio of the signal standard deviation and the overall standard deviation for the whole recording exceeded 1.3 were discarded from further analyses. Horizontal-to-vertical spectral ratios (HVSR) for each remaining window were computed as the ratio of the geometrical average of horizontal and the vertical Fourier amplitude spectra, smoothed with a Konno–Ohmachi window (Konno and Ohmachi 1998) with the *b*-parameter equal to 40. The spectra were finally stacked to obtain representative HVSR for each of the measurement points.

4 Results and interpretation

4.1 Comparison of observed HVSR with theoretical spectra

Selected typical HVSR measurements are shown in Fig. 4. along with the theoretical HVSR computed by ModelHVSR Matlab routines (Herak 2008) for the soil model defined in Sect. 2, and assuming that recorded noise is composed of body waves vertically incident from the halfspace. In most of the cases shown (with the exception of the point 29/15 located on the Bartolomija hill just beneath the Stoviš fortress on ground type A) the predominant period of the soil is clearly indicated at frequencies between 2.5 and 4.0 Hz. The theoretical, body-waves HVSR is seen to agree very well with the observed ones in most cases. Larger discrepancies in the amplitude of the main spectral peak are seen for points located to the south (e.g. 26/35, 29/12, 27/12E). However, even in these cases it is possible to obtain a good fit between observations and theoretical HVSR if the corresponding models are moderately adjusted. Fig. 5 shows two such cases, for the points 26/35 and 29/12E, for which the initial models were allowed to vary in ModelHVSR by up to 15 and 22%, respectively. Theoretical amplification spectra for P and S-waves, together with the HVSR for body waves for the best inverted model under the above constraints are shown in Fig. 5.

Ambient noise consists of a mixture of body-waves and surface waves, and it is of interest to compare observed HVSRs with theoretical ones also for surface waves. Which wave type prevails is still a matter of debate (see e.g. synthetic modelling by Bonnefoy-Claudet et al. 2006, 2008, or discussions by Nakamura 2000, 2009). Surface waves simulations were performed using the algorithm proposed by Lunedei and Albarello (2009), which is based on the assumption that the ambient vibrations wave field can be represented by the superposition of random multi-modal waves moving in all the directions at the surface of a flat layered visco-elastic Earth. These waves are assumed to correspond to Rayleigh and Love waves with their fundamental and higher modes generated by a distribution of random independent point sources located at the surface of the Earth and characterised by a uniform probability distribution all around the receiver. The method assumes plane waves and some other constraints (see Lunedei and Albarello 2009, for details). The effect of modal truncation presents an important problem. It is well known that strong seismic impedance contrasts increase the importance of higher surface wave modes in transferring

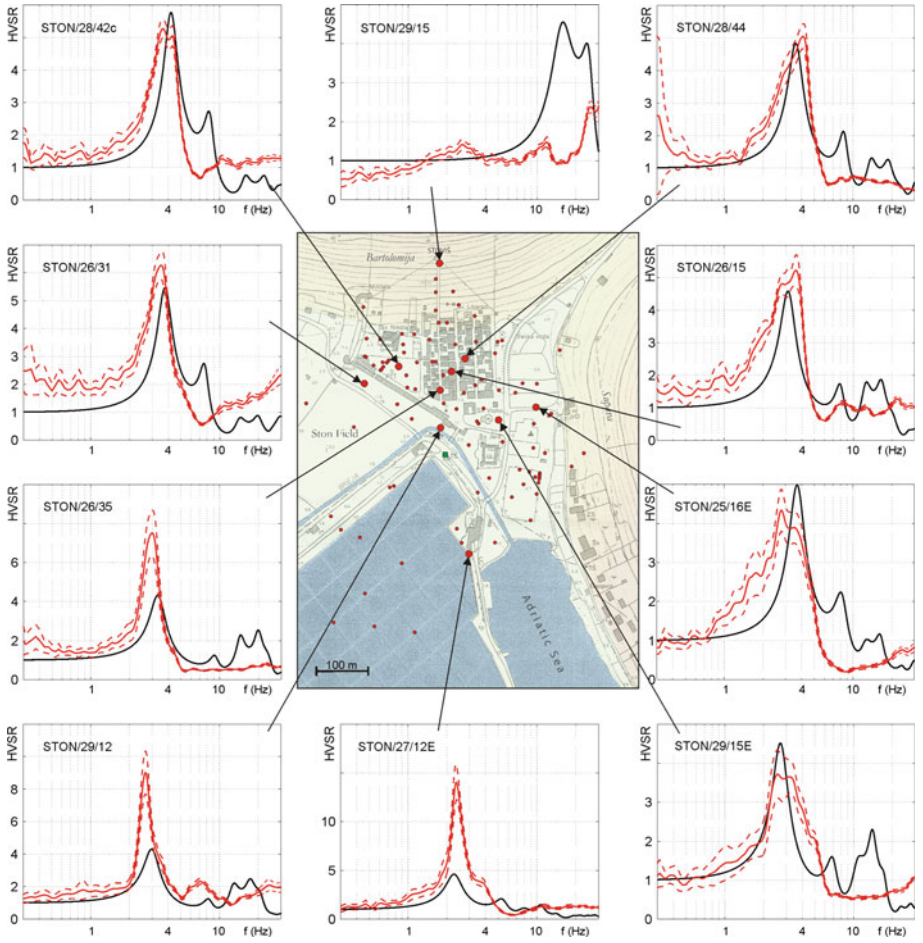

Fig. 4 Selected horizontal-to-vertical spectral ratios (HVSR). *Red* observed, ambient noise. 95% confidence limits are indicated by *red dashed lines*. *Black* Theoretical body-waves HVSR (see text for description of models). Note the variable vertical scale!

the seismic energy. Since propagation of these higher modes is conditioned by subsoil features at deeper depths with respect to those affecting the fundamental modes, their correct modelling requires artificial introduction of deep layers in the model to avoid unrealistic truncations of such modes. We have therefore extended our models to depths of 3000 m by adding layers that gradually increase velocities and densities to realistic values expected at such depths. Although arbitrary, such model extensions proved to produce reasonable results.

The simulations were done by considering the first 15 surface-wave modes for the two selected points and the corresponding best models found for body-waves by ModelHVSR. The resulting surface-waves HVSRs are shown in Fig. 5 (green lines).

It is seen that both methods reproduce observed HVSRs well, both in the location of the resonance frequency and regarding its amplitude and overall shape. It is also worth noting that observed HVSR is similar to the theoretical S-wave amplification spectrum around the soil fundamental frequency, but significant differences exist for the higher overtones, which are

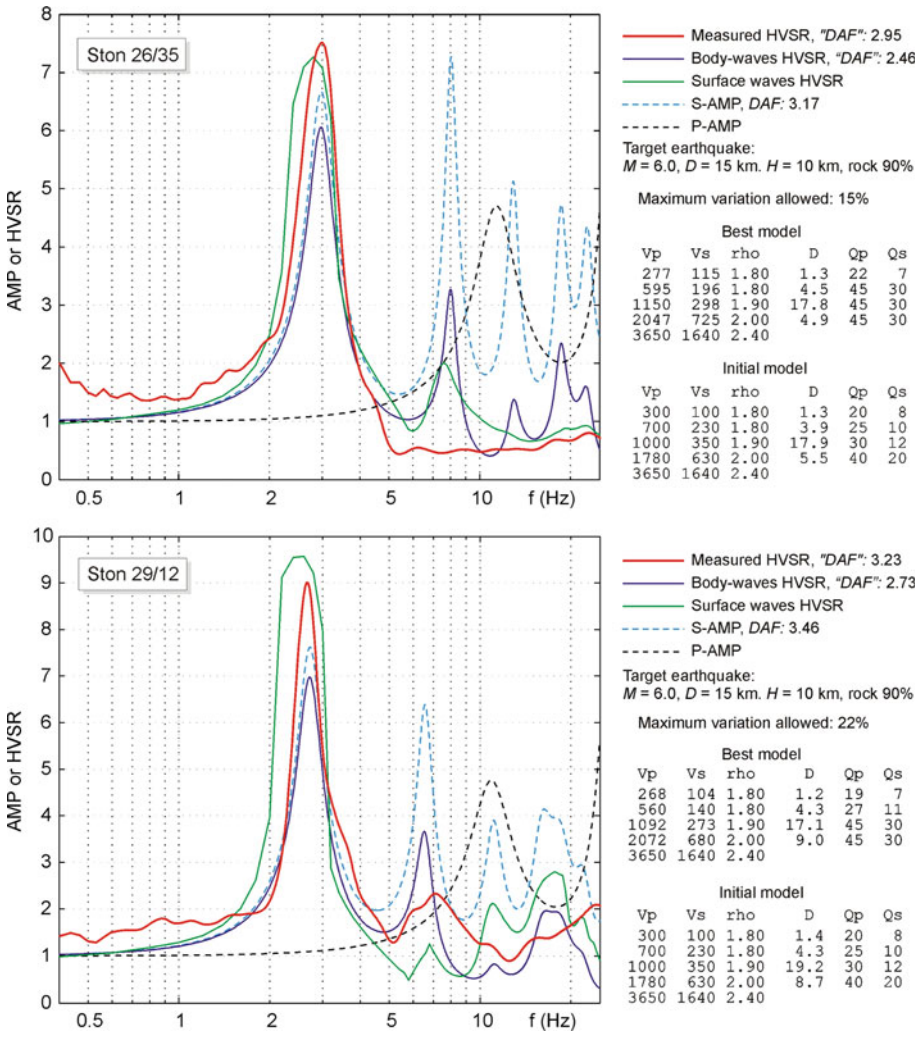

Fig. 5 Modelling of observed HVSR—examples for two measurement points showing: measured HVSR (*red*), theoretical body-waves HVSR (*blue*), theoretical surface-waves HVSR computed after Lunedei and Albarello (2009) for the first 15 modes and smoothed with a 5-point moving window (*green*), S-waves amplification spectrum (*light blue, dashed line*), P-wave amplification spectrum (*black, dashed line*). All theoretical spectra are for the final model which provides best fit of the observed HVSR. For the points 26/35 (*top*) and 29/12 (*bottom*) maximum allowed variation of depths and velocities were 15 and 22%, respectively. Amplification (DAF) values are computed for the target earthquake whose parameters are taken to represent the mainshock of 1996 ($M_L = 6.0$, epicentral distance = 15 km, depth of focus = 10 km, percentage of rock on the ray-path = 90%)

reduced in HVSR by division by the P-wave amplification spectrum (assumed to correspond to the vertical component of motion—see Herak 2008, for details). In the legend of Fig. 5 we also list the dynamic amplification factors (DAF) for the vertically incident S-waves, defined by Herak (2008) by invoking the Parseval's theorem and a well-known property from the random vibration theory that the maximum amplitude of a time series is proportional to its rms-value, as:

$$\mathrm{DAF} = \mathrm{PGA_s}/\mathrm{PGA_b} = \mathrm{rms}[A_\mathrm{b}(f)\mathrm{AMP_S}(f)]/\mathrm{rms}[A_\mathrm{b}(f)]. \quad (1)$$

Here PGA is the peak ground acceleration, subscripts s and b correspond to the surface and bedrock, respectively, $A_\mathrm{b}(f)$ is the acceleration Fourier spectrum at the bedrock level, and $\mathrm{AMP_S}(f)$ is the S-wave amplification spectrum. $[A_\mathrm{b}(f)\ \mathrm{AMP_S}(f)]$ is the Fourier spectrum of the surface acceleration. Note that DAF is in fact an integral measure of amplification depending not on the height of a single spectral peak, but on the whole amplification spectrum and on the expected spectrum of the incoming wave-field, $A_\mathrm{b}(f)$. Eq. 1 allows estimation of PGA amplification for a given soil model, provided $A_\mathrm{b}(f)$ is known for the target earthquake. Here, we estimate $A_\mathrm{b}(f)$ using empirical relations proposed by Trifunac (1993) and Lee and Trifunac (1995).

Dynamic amplification factors may also be formally defined for the HVSR-spectrum if it is inserted into (1) instead of $\mathrm{AMP_S}(f)$. For the theoretical HVSR, its value will always be somewhat lower than DAF for S-waves because $\mathrm{rms}(A_\mathrm{b} \times \mathrm{HVSR} = A_\mathrm{b} \times \mathrm{AMP_S}/\mathrm{AMP_P}) < \mathrm{rms}(A_\mathrm{b} \times \mathrm{AMP_S})$, but it may be a useful proxy if one has observations only (no theoretical model). This is especially so if the target event is of high magnitude and close to the site, so that non-linear soil response may be reasonably expected, for which linear amplification would yield unrealistically large values.

A good insight into all spectra obtained may be gained by HVSR-profiling, as shown in Figs. 6 and 7. In Fig. 6a we present HVSR profile running from the salterns in the south (A) to the Stoviš fortress (B) on the slopes of the Bartolomija hill. To produce the profile, only measurement points within 50 m of the AB line are considered (blue circles). The profile itself is a spatial spectrogram with distance along the profile on abscissa and frequency on the ordinate.

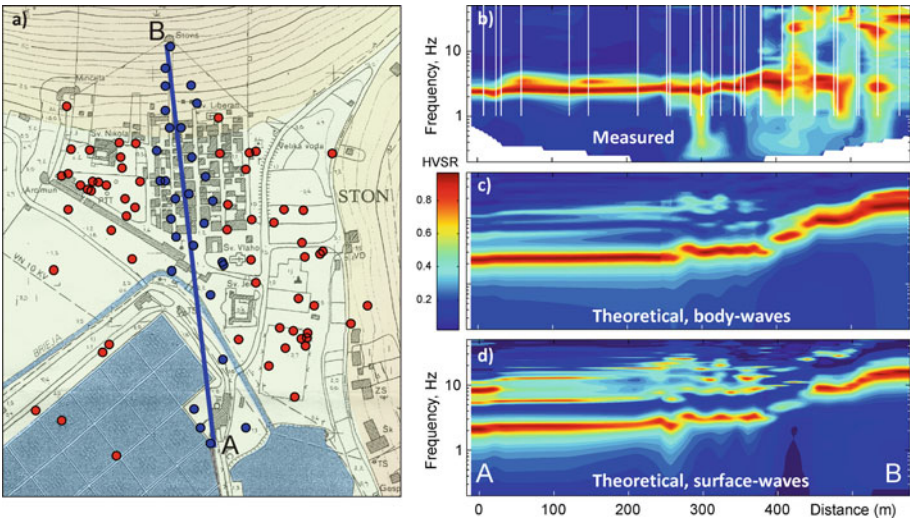

Fig. 6 **a** HVSR profile running from the salterns in the south (*A*) to the Stoviš tower in the north (*B*). Only points within 50 m from the profile trace (*blue*) are considered. **b** Smoothed HVSR profile obtained by gridding of the HVSRs (each normalized by its maximum) measured at places indicated by *white lines* in the top subplot. Relative amplitudes are colour-coded (see the colour-bar). **c** Theoretical normalized HVSR profile for body waves. **d** Theoretical normalized HVSR profile for surface waves. See text for details on the models and computational procedures

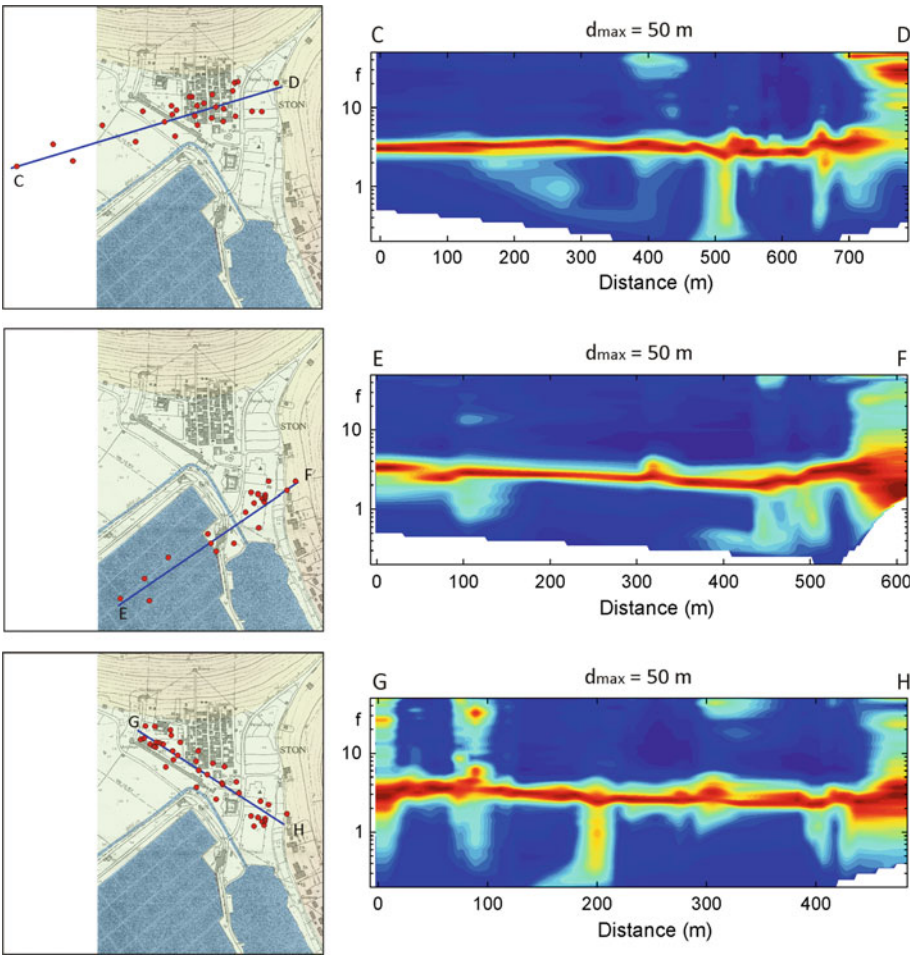

Fig. 7 Three selected observed HVSR profiles. For details see caption to Fig. 6

Normalized measured HVSR profile along the AB-line is shown in Fig. 6b, whereas the theoretical ones for body-waves and surface waves are presented in Fig. 6c, d, respectively. The three spectrograms agree almost perfectly in the flat terrain (the first 350 m) indicating a prominent spectral peak between 2 and 3 Hz. As the profile runs closer to the hill the observed frequency increases as the sedimentary cover starts to get thinner, which is indicated also in the theoretical profiles. Once the slopes of the Bartolomija hill are reached, observed HVSR gets "noisier" than the theoretical ones, with several equally prominent peaks at frequencies higher than 10 Hz, which is most probably caused by irregular layering and/or the topography. Just beneath the Stoviš fortress most of the energy is carried by the waves with frequencies above 20 Hz, well in agreement with theoretical predictions.

Figure 7 presents additional three HVSR profiles in various directions across the investigated area. All of them start in the west and end on the first slopes of the Supava hill, whose bedrock is clearly indicated close to point 'D'. In the profiles EF and GH the dominant frequency drops from 3.5 Hz at 'E' and 'G' to about 2 Hz 450 and 400 m away, respectively,

Fig. 8 Damage to buildings caused by the Ston-Slano earthquake of 1996. *Top left* St. Blasius church.*Bottom left* Ston Town Hall. *Top right* W–E running street. *Bottom right* S–N running street with the Stoviš tower in the background. Photographs by M. Herak, 1996

and then recovers. This is caused by a reduction of the shear wave velocity in the first layer by 25–35%, together with increase of soil thickness by about 20% with respect to other parts of profiles, as indicated by shallow seismic refraction results of Aleksovski et al. (1987). The reduction in the S-wave velocity may have to do with saturation of the top-most layers with water, as it is observed in the marshy area between the main road and the Supava hill. Known as *Velika voda* (meaning the "big water"), with a small creek flowing towards the sea, these wetlands have been partly reclaimed and are now used for parking, as a football field, for gardening, etc. Although S-wave velocity in soil is generally considered not to be much influenced by water saturation, experimental data and other studies (e.g. Iida 1938; Fratta et al. 2005; Adam et al. 2006; Lee and Collett 2006; Mondol et al. 2007) indicate that

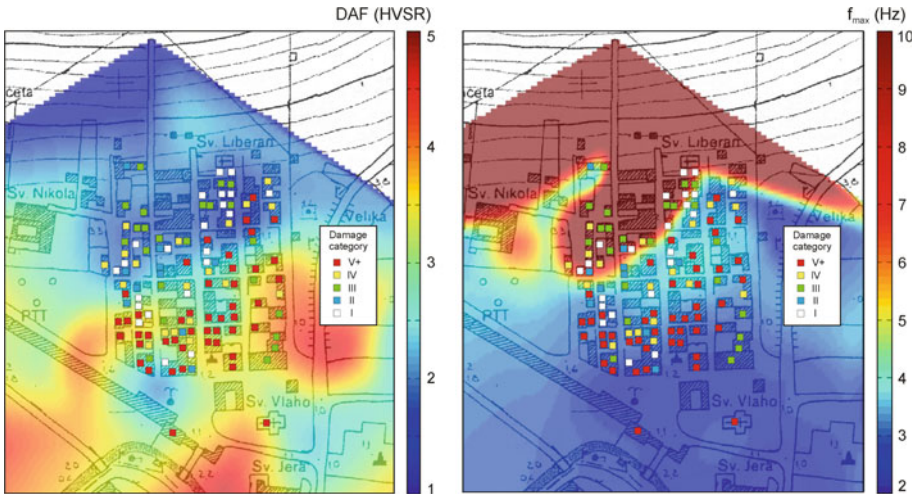

Fig. 9 Mapped values of amplification (DAF, *left*) and predominant frequency ($f_{\max}$, *right*) determined on the basis of measured HVSR spectra of ambient vibrations. $f_{\max}$ values are truncated at 10 Hz only for plotting

shear modulus may be sensitive to saturation with fluids due to weakening of the soil matrix. Increased water content may also lead to increase of bulk density, which also contributes to velocity decrease.

4.2 Comparison with observations from the Ston-Slano earthquake series of 1996

4.2.1 Macroseismic observations

The Ston-Slano earthquake series started with a mainshock (M_L=6.0) on September 5, 1996, whose epicentre was about 16 km to the SE. It was analysed in detail by Markušić et al. (1998), and Herak et al. (2001a) studied its aftershock sequence. The old city centre suffered the most severe damage—wide cracks in bearing walls (up to 10 cm wide), bulging and tilted walls, collapsed roofs and gables, etc. (Fig. 8). Most of inhabitants were moved to tents and trailers. The earthquake occurred just after the war-time scars of the city have been healed, and it is significant to note that no building renewed or re-erected after the war destruction (1991–1995) sustained any serious damage (Markušić et al. 1998).

After the earthquake authorities performed a detailed damage survey, classifying each building into seven categories, from 0 (no damage) to VI (total damage). Figure 9 presents assigned damage category superimposed on the map of DAF (based on the observed HVSR of ambient noise), and the frequency corresponding to the maximum of observed HVSR, which is in most cases the fundamental soil frequency. Although the pattern of damage is far from homogeneous (as is to be expected given quite diverse conditions the buildings were in when earthquake occurred), notably more severely damaged houses occurred in the southern and south-eastern parts of the town, where amplification (DAF) is the highest (between 2.5 and 3.5). The buildings close to or on the hill-slopes (DAF < 2) sustained mostly only moderate damage or remained unaffected. Similar picture emerges when the damage is compared to the soil predominant frequency, $f_{\max}$ (Fig. 9, right)—houses on soil with $f_{\max} > 8$ Hz were considerably less damaged than those in the flat land ($f_{\max} < 3.5$ Hz).

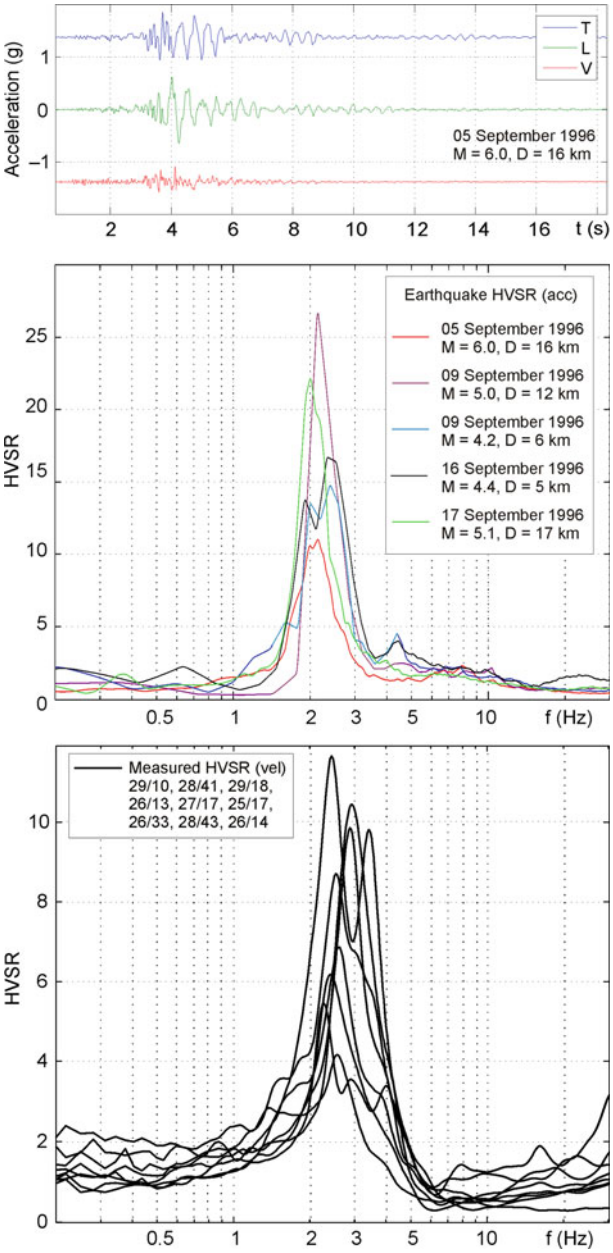

Fig. 10 *Top* Accelerograms of the Ston-Slano mainshock. *Middle* HVSR for the mainshock and the four aftershocks. Note that the peak at about 2.1 Hz is the smallest for the mainshock, indicating possible nonlinearity of soil response. *Bottom* HVSR of ambient noise at nine measurement points close to the accelerographic station

The houses in Ston are typical Dalmatian stone-masonry buildings, 2–4 storeys high. Almost all of them are built as parts of blocks, incorporating family houses and their gardens. In order to check if soil-structure resonance is also responsible for the observed

Table 3 Observed PGA (maximum of absolute value on any horizontal component) in Ston, and estimates of PGA on solid rock according to attenuation relationships by (Herak et al. 2001b, HMI) (Sabetta and Pugliese 1987, SP), and (Ambraseys et al. 2005, ADSS) for the mainshock and four aftershocks (Δ is epicentral distance)

Date	M_L	Δ (km)	Observed PGA (g)	PGA (HMI, g)	PGA (SP, g)	PGA (ADSS, g)	DAF (PGA)
5 Sep 1996	6.0	16	0.643	0.155	0.128	0.170	3.8–5.0
9 Sep 1996	5.0	12	0.178	0.088	0.072	0.113	1.6–2.5
9 Sep 1996	4.2	6	0.198	0.063	0.061	0.141	1.4–3.2
16 Sep 1996	4.4	5	0.257	0.076	0.080	0.176	1.5–3.4
17 Sep 1996	5.1	17	0.313	0.075	0.057	0.078	4.0–5.5

The last column gives the range of observed amplification of PGA with respect to estimated PGA (DAF = ratio between the observed PGA and the estimated one). All PGA in *g*

damage pattern, we performed five preliminary attempts to measure the dynamical parameters of such constructions using ambient vibrations. The results were rather poor (compared to those in reinforced-concrete buildings—e.g. Mucciarelli et al. 2009b), and it was difficult to confidently determine either the fundamental period or the damping. This implies that behaviour of such building blocks during shaking is poorly represented by harmonic oscillators, and that simple soil-structure resonance might not be the primary cause of damage. This is also in agreement with the observation that houses in the flat terrain (where the predominant noise frequency is low) were damaged more than those in the parts characterized with the higher soil frequencies, which must be closer to the fundamental frequency of the stone-masonry houses in Ston. Possible explanation may be that 'resonant' behaviour was induced by one of the higher soil overtones of AMP_S, which are seen in Fig. 5 to have considerable amplitude, but this is at the moment purely speculative and needs further studies.

4.2.2 Strong-motion recordings

The Ston-Slano earthquake of 1996 and several of its aftershocks were recorded by the accelerograph (Kinemetrics, SMA-1) which was located in the small doorkeeper's house at the entrance to the salterns (Fig. 1). The recording of the mainshock, reproduced in Fig. 10, is characterized by large accelerations on horizontal components, exceeding 0.64 g, and by relatively low predominant frequency of about 2 Hz. Table 3 lists magnitudes, epicentral distances and observed PGA for the mainshock and the four aftershocks, along with the PGAs predicted by the most commonly used attenuation relationships in Croatia. The last column gives the range of 'observed' DAF (the ratio between the measured and the predicted PGA), which clearly depends on the earthquake. Figure 10 also shows observed acceleration HVSRs for the five earthquakes and the ambient vibration HVSRs for the nine measurement points the closest to the accelerograph station. Similarity is clear, with the earthquake HVSRs having higher peaks on the average.

For the mainshock, the observed DAF is between 3.8 and 5.0 (depending on the reference attenuation relationship), which is in excellent agreement with the observed DAF from ambient vibrations in the vicinity of the accelerograph station (see Fig. 11).

5 Conclusions

Ambient vibrations measured in Ston provided results consistent with previous studies regarding soil structure. In particular, it was found that observed HVSR shapes are well matched

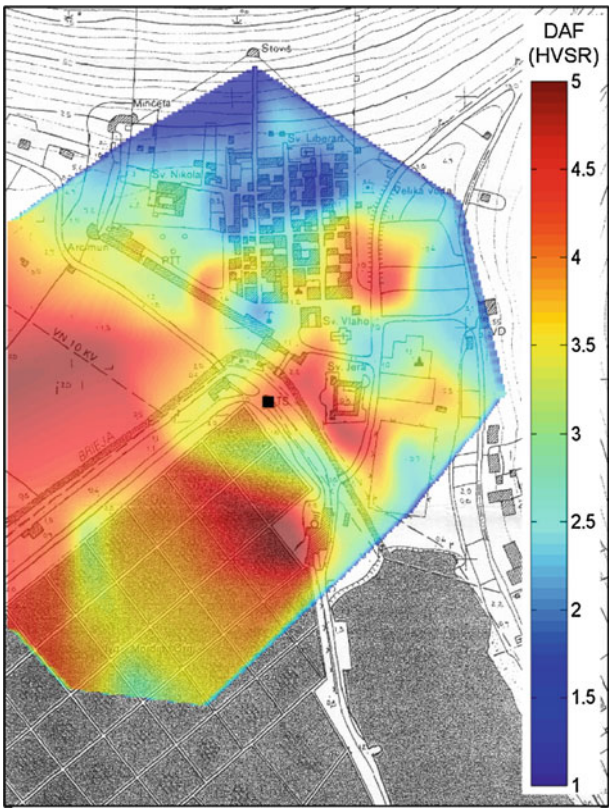

Fig. 11 Map of the observed DAF (first-order approximation estimate of PGA amplification) on the basis of HVSR of the ambient noise. Accelerographic station is shown by a *black square*

to the theoretical ones computed either for the body-waves or for the surface waves. This match was poorer for sites on the slopes of nearby hills, probably due to topographic effects and the sloping, thin, non-parallel layers.

The ratios of the measured peak horizontal acceleration during the mainshock and the ones obtained using empirical attenuation laws is approximately equal to the mapped DAF-value in the vicinity of the accelerometric station. The accelerogram HVSR is also very similar to the HVSR of the ambient noise.

The damage caused by earthquakes of 1996 to the building stock in the old town centre is well correlated with estimated soil amplification (DAF) determined on the basis of measured HVSR spectra.

Acknowledgments The study was done in the framework of the NATO SfP 980857 project, and was co-financed by the Ministry of Science, Education and Sports of the Republic of Croatia through the projects Nos. 119-1193086-1315 and 119-1193086-1314. We thank D. Albarello for providing a pre-release of the surface-waves simulation software, the mayor of Ston, V. Antunica, for the data on the earthquake damage, D. Uglešić from D&Z company (Zadar) for the borehole data, and Z. Milutinović and colleagues from IZIIS (Skopje) for the report on microzonation of Ston. We also thank two anonymous referees whose comments and constructive criticism helped us to improve the manuscript.

References

Adam L, Batzle M, Brevik I (2006) Gassmann fluid substitution and shear modulus variability in carbonates at laboratory seismic and ultrasonic frequencies. Geophysics 71:F173–F183. doi:10.1190/1.2358494

Aleksovski D, Arsovski M, Mirakovski G, Petkovski M, Kovačev P (1987) Seizmička mikrorajonizacija Stona. Geofizička istraživanja. Knjiga II. Izveštaj IZIIS 87-77. Institut za zemljotresno inženjerstvo i inženjersku seizmologiju Univerziteta Kiril i Metodij, Skopje

Ambraseys NN, Douglas J, Sarma SK, Smit PM (2005) Equations for the estimation of strong motions from shallow crustal earthquakes using data from Europe and Middle East: Horizontal peak ground acceleration and spectral acceleration. Bull Earthq Eng 3:1–53. doi:10.1007/s10518-005-0183-0

Bonnefoy-Claudet S, Cornou C, Bard P-Y, Cotton F, Moczo P, Kristek J, Fäh D (2006) H/V ratio: a tool for site effects evaluation. Results from 1-D noise simulations. Geophys J Int 167:827–837. doi:10.1111/j.1365-246X.2006.03154.x

Bonnefoy-Claudet S, Köhler S, Cornou C, Wathelet M, Bard P-Y (2008) Effects of Love Waves on Microtremor H/V Ratio. Bull Seismol Soc Am 98:288–300. doi:10.1785/0120070063

Cara F, Cultrera G, Azzara RM, De Rubeis V, Di Giulio G, Giammarinaro MS, Tosi P, Vallone P, Rovelli A (2008) Microtremor Measurements in the City of Palermo, Italy: Analysis of the Correlation between Local Geology and Damage. Bull Seismol Soc Am 98:1354–1372. doi:10.1785/0120060260

Chatelain JL, Guillier B, Cara F, Duval A-M, Atakan K, Bard P-Y, the WP02 SESAME team (2008) Evaluation of the influence of experimental conditions on H/V results from ambient noise recordings. Bull Earthq Eng 6:33–74. doi:10.1007/s10518-007-9040-7

D'Amico V, Picozzi M, Baliva F, Albarello D (2008) Ambient Noise Measurements for Preliminary Site-Effects Characterization in the Urban Area of Florence, Italy. Bull Seismol Soc Am 98:1373–1388. doi:10.1785/0120070231

Elnashai A, Di Sarno L (2008) Fundamentals of earthquake engineering. Wiley, Chichester, p 347

Fratta D, Alshibli KA, Tanner WM, Roussel L (2005) Combined TDR and P-wave velocity measurements for the determination of in situ soil density—experimental study. Geotech Test J 28:1–11. Available online. www.astm.org, Accessed 8 April 2009

Geotehnički studio (2005) Crkva svetog Vlaha u Stonu. Geotehnički elaborat. Zagreb, p 13 (in Croatian)

Gosar A (2007) Microtremor HVSR study for assessing site effects in the Bovec basin (NW Slovenia) related to 1998 M_W5.6 and 2004 M_W5.2 earthquakes. Eng Geol 91:178–193. doi:10.1016/j.enggeo.2007.01.008

Gosar A, Martinec M (2009) Microtremor HVSR study of site effects in the Ilirska Bistrica Town Area (S. Slovenia). J Earthq Eng 13:50–67. doi:10.1080/13632460802212956

Hasancebi N, Ulusay R (2006) Evaluation of site amplification and site period using different methods for an earthquake-prone settlement in Western Turkey. Eng Geol 87:85–104. doi:10.1016/j.enggeo.2006.05.004

Havenith H-B, Fäh D, Polom U, Roullé A (2007) S-wave velocity measurements applied to the seismic microzonation of Basel, Upper Rhine Graben. Geophys J Int 170:346–358. doi:10.1111/j.1365-246X.2007.03422.x

Herak M (2008) ModelHVSR—A Matlab® tool to model horizontal-to-vertical spectral ratio of ambient noise. Comput Geosci 34:1514–1526. doi:10.1016/j.cageo.2007.07.009

Herak M, Herak D, Markušić S (1996) Revision of the earthquake catalogue and seismicity of Croatia, 1908–1992. Terra Nova 8:86–94. doi:10.1111/j.1365-3121.1996.tb00728.x

Herak M, Herak D, Markušić S, Ivančić I (2001a) Numerical modelling of the Ston-Slano (Croatia) aftershock sequence. Stud Geophys Geod 45:251–266. doi:10.1023/A:1022032128687

Herak M, Markušić S, Ivančić I (2001b) Attenuation of peak horizontal and vertical acceleration in the Dinarides area. Stud Geophys Geod 45:383–394. doi:10.1023/A:1022077603943

Iida K (1938) The velocities of elastic waves in sand. Bull Earthq Res Inst XVI:131–144

Konno K, Ohmachi T (1998) Ground-motion characteristics estimated from spectral ratio between horizontal and vertical components of microtremor. Bull Seismol Soc Am 88:228–241

Lachet C, Hatzfeld D, Bard P-Y, Theodulidis N, Papaioannou C, Savvaidis A (1996) Site effects and microzonation in the city of Thessaloniki (Greece) comparison of different approaches. Bull Seismol Soc Am 86:1692–1703

Lee MW, Collett TS (2006) Gas hydrate and free gas saturations estimated from velocity logs on Hydrate Ridge, offshore Oregon, USA. In: Tréhu AM, Bohrmann G, Torres ME, Colwell FS (eds) Proc. ODP, Sci. Results 204:1–25. Available online. www.odp.tamu.edu/publications/204_SR/VOLUME/CHAPTERS/103.PDF, Accessed 4 April 2009

Lee VW, Trifunac MD (1995) Frequency dependent attenuation function and Fourier amplitude spectra of strong earthquake ground motion in California. University of Southern California, Los Angeles, USC Report No. CE 95-03, 190 pp

Lunedei E, Albarello D (2009) On the seismic noise wavefield in a weakly dissipative layered earth. Geophys J Int Available on-line. http://dx.doi.org/10.1111/j.1365-246X.2008.04062.x

Markušić S, Herak D, Ivančić I, Sović I, Herak M, Prelogović E (1998) Seismicity of Croatia in the period 1993–1996 and the Ston-Slano earthquake of 1996. Geofizika 15:83–102

Mondol NH, Bjørlykke K, Jahren J, Høeg K (2007) Experimental mechanical compaction of clay mineral aggregates—changes in physical properties of mudstones during burial. Mar Pet Geol 24:289–311. doi:10.1016/j.marpetgeo.2007.03.006

Mucciarelli M, Herak M, Cassidy J (eds) (2009a) Increasing seismic safety by combining engineering technologies and seismological data. NATO Science for Peace and Security Series, Springer, Dordrecht, p 382

Mucciarelli M, Gallipoli MR, Gosar A, Šket-Motnikar B, Rošer J, Zupančič P, Prevolnik S, Herak M, Stipčević J, Herak D, Milutinović Z, Olumčeva T (2009b) Empirical estimates of dynamic parameters on a large set of European buildings. Bull Earthq Eng (Submitted)

Nakamura Y (1989) A method for dynamic characteristics estimation of subsurface using microtremor on the ground surface. Q Rep Railw Techn Res Inst 30:25–33

Nakamura Y (2000) Clear identification of fundamental idea of Nakamura's technique and its applications. In: Proceedings of the 12th World Conference on Earthquake Engineering, New Zealand CD-ROM, 8 p

Nakamura Y (2009) Basic structure of QTS (HVSR) and examples of applications. In: Mucciarelli M, Herak M, Cassidy J (eds) Increasing seismic safety by combining engineering technologies and seismological data. NATO Science for Peace and Security Series, Springer, Dordrecht, pp 33–51

Panou AA, Theodulidis N, Hatzidimitriou P, Stylianidis K, Papazachos CB (2005) Ambient noise horizontal-to-vertical spectral ratio in site effects estimation and correlation with seismic damage distribution in urban environment: the case of the city of Thessaloniki (Northern Greece). Soil Dyn Earthq Eng 25:261–274. doi:10.1016/j.soildyn.2005.02.004

Sabetta F, Pugliese A (1987) Attenuation of peak horizontal acceleration and velocity from Italian strong-motion records. Bull Seismol Soc Am 77:1491–1513

Scherbaum F, Hinzen K-G, Ohrnberger M (2003) Determination of shallow shear wave velocity profiles in the Cologne, Germany area using ambient vibrations. Geophys J Int 152:597–612. doi:10.1046/j.1365-246X.2003.01856.x

Trifunac MD (1993) Broad band extension of Fourier amplitude spectra of strong motion acceleration, University of Southern California, Los Angeles,USC Report No. CE 93-01, 109 pp